Independent computation of the 2D Boussinesq corner blowup profile: the scaling exponent, an eigenvalue-free stability certificate, and a free-residual test that catches a false root

J. Hill

28 July 2026

Abstract

We compute the self-similar blowup profile of the 2D Boussinesq system in a corner domain, the object underlying the Luo–Hou scenario for 3D axisymmetric Euler with boundary, by a route independent in discretization, formulation and solver from both existing computations. The profile is solved as a root problem with an explicit sparse Jacobian, rather than by marching or by neural approximation. We obtain $\alpha = -0.34240 \pm 4.4 \times 10^{-5}$, consistent with the cross-method reference value -0.34240009, which is itself agreed on by an adaptive-mesh march and a physics-informed network to 3.4×10^{-7}. The free gauge residual, a functional the solve is answerable to nothing for, closes to 1.8×10^{-6} on the quoted ladder and to 8.7×10^{-7} at the deepest corner resolution reached.

Our independence is not total, and we state the exception precisely: two scalar corner constants, W_x and Θ_{xx}, are read off the reference profile and imposed as gauge targets, and the interior seed of the production ladder is interpolated from the same profile. We show the *seed* dependence is immaterial (Section 4.2) and that the *corner constants* are not: freeing one of them moves α by 9.7×10^{-5}, about twice the quoted bar. This is a genuine shared input, not an independent check, and the note treats it as such throughout.

Three further results are, to our knowledge, new. First, the corner-regularized system possesses an exact one-parameter scaling symmetry under which α is invariant; we verify it symbolically and confirm on the converged root that the Jacobian annihilates its generator on every covariant row to 2.8×10^{-12}. Second, we certify linear stability of the profile *without trusting any eigenvalue*, by a Lyapunov certificate on the descriptor realization whose verification reduces to an absolute inequality; in the same section we show the rightmost eigenvalue of this operator is unconverged as a discretization at both resolutions computed, agreeing between two solution routes to 7.2×10^{-9} while disagreeing between two grids by 2.1×10^{-1}. Third, we report a *false* root: a state converging to $\|F\| = 5.4 \times 10^{-14}$, distinct from the ground state, stable under wedge truncation, and morphologically coherent, which is nevertheless an artifact of the pinned discretization. We give the one-line diagnostic that separates it from the true profile at three orders of magnitude, and argue that residual, distinctness, parameter stability and morphological coherence are jointly insufficient to certify a self-similar profile.

1 The object and the prior art

The Luo–Hou scenario [6] proposes finite-time blowup for 3D axisymmetric Euler with a solid boundary, driven by a hyperbolic point on the wall. Its 2D Boussinesq analogue admits a self-similar reduction whose profile satisfies a nonlinear elliptic system in a corner. The quantity of interest is the scaling exponent α, which fixes the temporal rate of the blowup.

Two computations of this profile exist. Chen and Hou [1, 2, 3] solve it by an adaptive-mesh march with a slaved gauge, in the line of work supporting a computer-assisted proof. Wang and collaborators [4] solve it with a physics-informed network refined by Gauss–Newton [5]. The two share neither discretization nor solution strategy, and they agree on α to 3.4×10^{-7}, which is why we treat $\alpha_{\text{ref}} = -0.34240009$ as a reference rather than as a competitor.

What has been missing is a third route with a different failure mode. A march accumulates error along its direction of integration; a network's error is opaque to the practitioner. A root problem with an explicit Jacobian fails in neither of those ways. It fails by rank deficiency, by inconsistency, or by converging to the wrong object, all of which are detectable by linear algebra on matrices one can inspect. Sections 3 and 7 are, respectively, an instance of the second failure mode and an instance of the third, both caught by that inspection.

2 Formulation

2.1 Corner regularization

In the corner frame $\xi = \ln(1 + r)$ with β the angular variable on the wedge, the natural unknowns carry algebraic prefactors at the corner. Working with them directly produces transport rows that are $O(\xi)$-scaled near the wall, with the consequences documented in Section 3.1. We instead substitute globally

$$\tilde{\Omega} = \xi A, \qquad \tilde{B} = \xi^2 B, \qquad \tilde{\Psi} = \xi^2 P,$$

and divide the three residuals by ξ, ξ^2, ξ^2, performing every cancellation analytically rather than in floating point. Writing $G_1 = -\text{expm1}(-\xi)/\xi$ (analytic, $G_1(0) = 1$) and $E_1 = e^{a_0 \xi}/G_1$, and bundling the first-order operators as

$$L_A = I + X(D_\xi + a_0 I), \qquad L_{B2} = 2I + X\big(D_\xi + (1 + 2a_0)I\big), \qquad L_{P\mu} = 2I + X(D_\xi + \mu I),$$

the divided residuals are exact identities. Three consequences follow, each closing a failure mode of the undivided formulation. The corner circle $\xi = 0$ now carries real equations rather than imposed identities. The wall-line rows are $O(1)$ instead of $O(\xi)$. And the gauge constraints become single-entry value pins in place of derivative functionals whose conditioning grew as N^4.

2.2 Panels, and the decision that made the Jacobian sparse

The radial direction is discretized by piecewise-Chebyshev panels with duplicated interface nodes and classical patching: C^0 matching for the transport equations, C^0 and C^1 for the Poisson equation.

The load-bearing choice is to keep $\tilde{\Psi}$ as an *unknown* rather than eliminating it by a Poisson solve. Elimination is the obvious move and it is a trap: it makes every operator nonlocal, so the

Jacobian is dense at any grid size, and each Jacobian column costs a Poisson solve. Retaining $\tilde{\Psi}$ keeps every operator local and the exact Jacobian sparse. Every diagnostic in this note is a sparse factorization, so every result below depends on that choice.

2.3 Gauge closure and the free residual

The scalars c_ℓ, c_w are closed by two gauge functionals evaluated at the corner, with targets $W_x = 1.19620314$ and $\Theta_{xx} = 1.79819132$ read from the reference profile. These two numbers are the note's one substantive shared input with prior work, and Section 4.3 measures what they cost.

This closure leaves a functional *unused*, and it is the most valuable object in the computation. The continuum corner algebra forces

$$c_\ell = \frac{2\Theta_{xx}}{W_x} = 3.00649824,$$

and nothing in the discrete system imposes it. We therefore define the **free residual**

$$h_{\mathrm{id}} \;=\; c_\ell - \frac{2\Theta_{xx}}{W_x},$$

report it beside every converged solution, and treat it as the primary certificate. It is answerable to no tuning. Section 7 is the argument that a computation of this kind should not be believed without such a functional.

3 Two mechanisms found along the way

3.1 Corner dust

Transport rows collocated at wall nodes with $\xi \lesssim 0.025$ are near-vacuous: in the undivided formulation their entries are $O(\xi)$-scaled and drown in roundoff. The rows go dependent and the system becomes rank-deficient and inconsistent.

This single threshold is consistent with a family of failures previously recorded as unrelated: the dense solver's ceiling at $N \approx 52$ to 56, the failure at panel length $L = 10$, and an outlier at $N = 52$, all of which satisfy "the first radial node falls below $\xi \approx 0.025$" while the successful configurations do not. The regularization above removes the mechanism rather than avoiding it.

3.2 The wedge truncation carries a singular layer

Computations on this domain truncate the wedge by ε_b, replacing the opening $\pi/2$ with $\pi/2 - 2\varepsilon_b$. This is not a small perturbation of the boundary condition. It shifts the corner exponent to

$$k \;=\; \frac{\pi}{\pi/2 - 2\varepsilon_b},$$

so that $P = \tilde{\Psi}/\xi^2$ carries a weakly singular layer ξ^{k-2} that no polynomial radial basis represents. At $\varepsilon_b = 10^{-3}$, $k = 2.002550$.

The observable consequence is sharp and was initially baffling. Coarse corner panels cannot resolve the misfit and converge normally. Once the first radial node drops below roughly 0.012, the layer is resolved and we can find no root: the residual floors at 8×10^{-5} to 1.4×10^{-4} with every Newton step accepted and the residual immobile, for two independent solvers. Reducing ε_b to 10^{-4} removes the floor entirely and the same configurations converge in three to four Newton steps.

This is worth stating plainly, because the symptom, a residual floor with accepted steps, is easily misread as a solver defect. It is a statement about the truncated problem.

4 The exponent

4.1 The ladder and the quoted value

At degs $= (24, 56, 12)$, $N_\beta = 36$:

ε_b	α	h_{id}/c_ℓ	$\|F\|$
1.0×10^{-4}	-0.34541032	$+2.6 \times 10^{-5}$	9.4×10^{-13}
5.0×10^{-5}	-0.34386167	$+1.4 \times 10^{-5}$	6.4×10^{-12}
2.5×10^{-5}	-0.34312079	$+7.1 \times 10^{-6}$	5.3×10^{-12}
1.0×10^{-5}	-0.34268591	$+3.2 \times 10^{-6}$	3.9×10^{-12}
5.0×10^{-6}	-0.34254247	$+1.8 \times 10^{-6}$	7.3×10^{-12}

The free residual is reported relative to c_ℓ; it falls monotonically to 1.8×10^{-6}. At corner degree 28 and $\varepsilon_b = 5 \times 10^{-6}$ it reaches 8.7×10^{-7}, with α moving by 9.8×10^{-6}.

Extrapolating to $\varepsilon_b \to 0$ requires choosing a model class, and we decline to choose. Three families fit the five-rung ladder with residuals we cannot distinguish on five points (Figure 1):

model	$\alpha(0)$	deviation from reference
$a + b\varepsilon$	-0.34237665	$+2.3 \times 10^{-5}$
$a + b\varepsilon + c\varepsilon^2$	-0.34240048	-3.9×10^{-7}
$a + b\varepsilon + c\,\varepsilon \ln \varepsilon$	-0.34241599	-1.6×10^{-5}

Their spread is 3.93×10^{-5} about a midrange of -0.34239632. Since the singular layer of Section 3.2 has exponent $k - 2 \sim \varepsilon_b$, a non-polynomial term is physically plausible and the polynomial fit cannot be preferred on principle. Adding in quadrature the measured corner-degree systematic of Section 4.2 (1.94×10^{-5}) gives the quoted bar:

$$\boxed{\alpha = -0.34240 \pm 4.4 \times 10^{-5}}$$

We note, without adopting it, that the extrapolation stabilizes as the coarsest rungs are dropped: the linear and quadratic fits differ by 2.4×10^{-5} on all five rungs, 7.2×10^{-6} on the deepest four, and 2.5×10^{-6} on the deepest three. Quoting the deepest-three bar would report agreement at 2.5×10^{-6}. We do not, because choosing the subset that tightens the bar is the same error as choosing the model family that does.

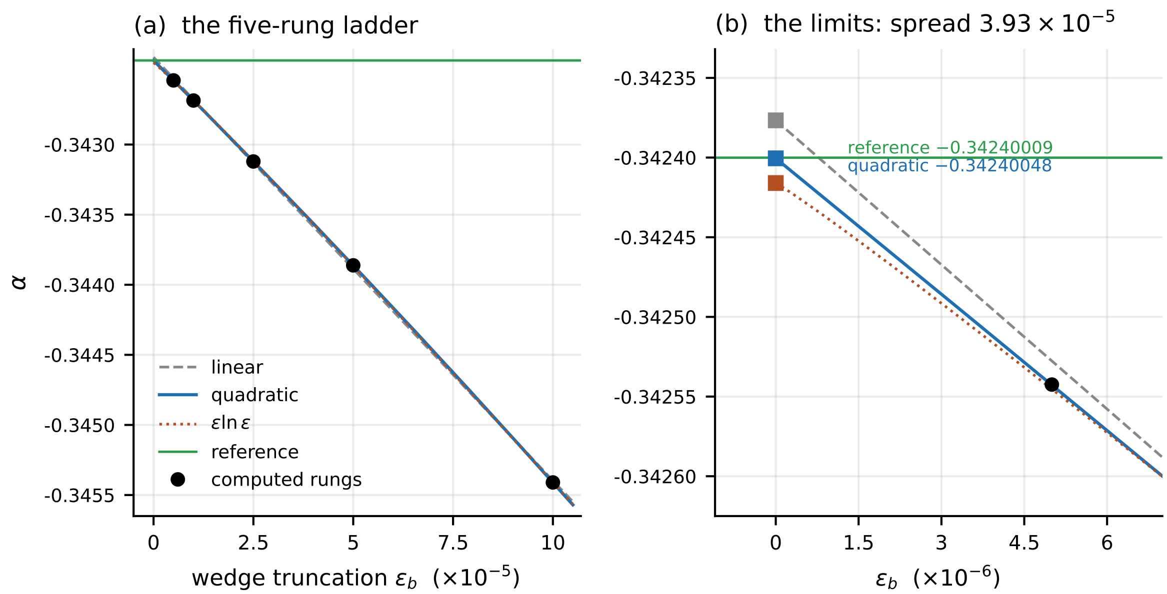

Figure 1: The five-rung ε_b ladder (a) and, resolved in (b), the 3.93×10^{-5} spread between the three extrapolation families at $\varepsilon_b \to 0$, against the cross-method reference value. Every plotted point is a converged solve.

4.2 Which axes were probed, and how far

axis	worst effect on α	status
N_β, $36 \to 48$	1.16×10^{-8}	closed
seed provenance	9.65×10^{-8}	closed
axis-column pinning	3.0×10^{-8}	closed
far-field truncation, $X_{\max}$ $25 \to 32$	1.45×10^{-10}	closed
middle panel edge, $15 \to 18$	1.45×10^{-10}	closed
corner degree, $24 \to 28$	1.94×10^{-5}	in the bar
corner degree, $16 \to 24$	6.98×10^{-4}	not converged at 16
ε_b truncation	extrapolated, layer analysed	in the bar

Two entries need comment.

The seed row closes the last hidden constant. Every configuration in the production ladder seeded its interior field by interpolating the reference profile, and agreement among configurations is structurally blind to anything they all share. We re-solved from three *purely analytic* seeds carrying no reference data in the interior, namely the corner limits times $e^{-\xi/L}$ for $L = 2, 4, 8$, obtaining deviations 9.7×10^{-8}, 7.8×10^{-8} and 6.9×10^{-8} with a spread among themselves of 2.7×10^{-8}. The $L = 1$ seed did not converge, terminating with zero accepted Newton steps, which we report as a basin observation. These runs were performed at a configuration where α itself is about 0.7% from the extrapolated value, so they bound the seed sensitivity of the *root found*, not of the extrapolated exponent.

The far-field and panel-edge rows were the final open axes. Moving the far field from $X_{\max} = 25$ to 32, and independently moving the middle panel edge from 15 to 18, changes α

by 1.45×10^{-10} in both cases, five orders below the quoted bar. We verified the interventions were real rather than ignored: the radial node sets differ by 7.0 and 3.0 respectively, so the insensitivity is a property of the solution and not of the driver.

4.3 What the shared corner constants cost

Freeing Θ_{xx} as an unknown and closing the system with the corner identity (the experiment of Section 7.3, which fails for an unrelated reason) moves the converged α by 9.73×10^{-5}, about twice the quoted bar. The gauge targets are therefore a real shared input with Chen and Hou, and this note claims independence of *method*, not of *data*.

5 The exact scaling symmetry

The divided residuals are covariant under

$$A \to sA, \quad B \to s^2 B, \quad P \to sP, \quad c_\ell \to s\, c_\ell, \quad c_w \to s\, c_w,$$

with $R'_\Omega \to s^2 R'_\Omega$, $R'_B \to s^3 R'_B$, $R'_P \to sR'_P$. The grading $(1, 2, 1, 1, 1)$ is the unique solution; the system is *not* homogeneous under field scaling alone, and the compensating rescale of (c_ℓ, c_w) is what makes $\alpha = c_w/c_\ell$ **invariant**.

Verification is at two levels. Symbolically the identities hold exactly. On the coded solver at a random state, all 896 covariant rows scale with their derived exponent to 1.348×10^{-15}, and the Euler check $Jv = d\,F$ holds to 1.011×10^{-15}; the only rows that break covariance are the static pins and gauge targets, and their breakage equals $(s^k - 1) \times$ field to 4.441×10^{-16}, as predicted.

At a converged root the consequence is structural. Euler's identity gives $DR \cdot v = d\,R$ for a row of degree d, and $R = 0$ at a root, so $Jv = 0$ on every covariant row. Measured on the converged profile with generator $v = (A, 2B, P, c_\ell, c_w)$:

$$\|Jv\|_{\text{covariant}} = 2.814 \times 10^{-12}, \qquad \frac{\|Jv\|_{\text{pins+gauge}}}{\|Jv\|} = 100.0000\%.$$

The symmetry is therefore the dominant soft direction of the Jacobian at the solution: $\sigma_{\min}(J) = 2.536 \times 10^{-6}$, with the soft mode 68.9% aligned with v. The gauge rows suppress its c_ℓ, c_w components to 0.305 and 0.646 of the predicted values, which is why the mode presents in parameter sweeps as "c_ℓ, c_w nearly fixed" and was for some time misread as such.

6 Linear stability, without trusting an eigenvalue

6.1 The realization

The stability operator is not the Jacobian of the steady system. In the divided variables the exponential factors are independent of the self-similar time, so the mass matrix on the two transported blocks is the identity and the linearization is a **descriptor pencil** (E, J) with J the solver's own Jacobian unmodified and E a 0/1 diagonal mask, equal to 1 exactly on live transport rows. Everything else, the pins, the interface matching, the Poisson block, the two gauge rows and the two scalar columns, is algebraic. The pencil has Hessenberg index

2. On a reduced structural configuration ($N = 722$) a QZ count returns 376 finite and 346 infinite eigenvalues, the infinite count matching $(N - \operatorname{rank} E) + m$ exactly, and the compressed generator agrees with the pencil to 3.7×10^{-10}.

The admissible state space is $\ker C_g$. Restricting to it removes the grading direction *by construction*:

$$\sigma_{\min}(J) = 2.5356 \times 10^{-6} \longrightarrow \sigma_{\min}\left(L\big|_{\ker C_g}\right) = 3.9701 \times 10^{-3},$$

a factor of 1565.7, reproduced at three roots (1565.7, 1724.0, 1529.1; these roots have $\alpha = -0.34471$, -0.34541, -0.34349, none of them the quoted extrapolated value) with gauge leakage $\|C_g w\|/\|w\| = 3.9 \times 10^{-17}$.

We record a negative result about our own first instinct. Deflating the grading direction explicitly, which we expected to be necessary, is *wrong* rather than redundant. Its restricted shadow is an ordinary stiff direction of the generator, $\|Lw_1\|/\|w_1\| = 12.08$, about 1% of $\|L\|$ and $3043\times$ $\sigma_{\min}(L)$, and deflating it moves the resolvent norm in the right half plane by 19.6%.

6.2 The certificate

Since Section 6.3 shows this operator's eigenvalues are unconverged, we certify stability without them. Solving $L^{\mathsf{T}}P + PL = -I$ by Bartels–Stewart gives relative residuals 4.85×10^{-16}, 4.88×10^{-16}, 4.68×10^{-16} at three roots, with $\operatorname{chol}(P)$ succeeding at all three.

We are explicit that Bartels–Stewart computes a real Schur decomposition internally, so the route is not eigenvalue-free as an *algorithm*. It is eigenvalue-free as a *certificate*, and the distinction is the point: verification does not require trusting the Schur output, because the residual bound

$$\|E\|_2 \leq 4.85 \times 10^{-16}\, \lambda_{\max}(P)\, \|L\| = 3.06 \times 10^{-8} < 1$$

makes $P \succ 0$ with $L^{\mathsf{T}}P + PL \prec 0$ an inequality checkable independently. Hurwitz-ness follows from that inequality, not from any computed eigenvalue.

The companion pseudospectral statement is that no ε-pseudospectrum reaches $\operatorname{Re} z > 0$ below $\varepsilon^* = 3.93 \times 10^{-3}$ at the first resolution and 3.08×10^{-3} at the second, against a round-off floor $n\varepsilon_{\text{mach}}\|L\| = 1.175 \times 10^{-9}$. We quote the *worst* margin, 8.8×10^5. The right-half-plane minimum sits on the imaginary axis (3.946×10^{-3} against 8.984×10^{-3} over the interior), as Davies–Shargorodsky requires. The verdict survives the refinements available: N_β from 36 to 28 moves the spectral abscissa by 1.56×10^{-6} and $X_{\max}$ from 25 to 18 by 3.36×10^{-5}. The ε^* level does not survive, moving 21.5% across corner degrees, and is quoted with that band.

One caveat is structural rather than numerical: the untruncated essential spectrum of this operator sits on the imaginary axis, so ε^* should be expected to shrink as $X_{\max}$ grows. Our $X_{\max}$ pair above is a coarsening rather than a refinement, and the behaviour of ε^* under genuine far-field refinement is untested.

Transient growth is genuine: $89.7 \leq \sup_t \|e^{tL}\| \leq 5807.6$ at the first resolution and 148.7 to 7973.8 at the second, in the raw collocation norm, which is not similarity-invariant and is labelled as such.

Two quantities that look like physics are not. A single-dominant-block model of L predicts $\omega(L)/\|L\| = 1/2$ exactly, and we measure 0.4952, 0.4967, 0.4952; the closed form $e^{a_0\xi}\xi/2$ matches to 5.140972×10^{-1} against 5.140981×10^{-1}, and zeroing that block caps the maximum real part at $+15.68$. And the essential numerical range of the corner-regularized symbol is $\mathbb{C}$, not the imaginary axis: $\max \operatorname{Re} W(S) = +5.14 \times 10^4$ at $k = 10^5$ and $+5.14 \times 10^5$ at $k = 10^6$, growing linearly. Spectral pollution confinement is vacuous in this norm. This retracts a closed-form essential-numerical-range claim made earlier in this project.

6.3 What is not converged, and what is not claimed

The rightmost eigenvalue is agreed on by two independent computational routes to 7.2×10^{-9} (worst of two roots), and disagrees between two grids by 2.1×10^{-1}, changing character from a complex pair to a real value. Seven and a half orders of magnitude separate "well-posed as linear algebra" from "converged as discretization." The eigenvalue condition numbers are 1.1×10^3, 2.3×10^3, 1.5×10^3. We report no eigenvalue, and we state the negative in the form the evidence supports: unconverged as a discretization at the two resolutions computed, not unmeasurable in principle.

We do not claim unconditional linear stability. The Lyapunov rate 8.82×10^{-6} lies 3.6×10^4 below the Schur abscissa 3.17×10^{-1}: Hurwitz means no right-half spectrum, not decay at a rate. The admissible class is corner-clamped, since the corner pin removes the continuum two-dimensional corner ODE from the realization and the axis column imposes an extra Dirichlet condition on the perturbation whose spectral cost we have not measured. The claim is Hurwitzness of the corner-clamped linearization at two resolutions, in the raw collocation norm, at fixed ε_b on a truncated wedge, and nothing larger.

7 A false root

The following is reported because we believe it is the most transferable content in this note.

7.1 What it passed

Searching for unstable branches, we froze the exponent at a published unstable value and searched *field* space by deflation. One start in eight, at half the ground state's amplitude, converged to a state with $\|F\| = 5.4 \times 10^{-14}$ at relative distance 1.70 from the ground state. It passed three independent checks. It satisfied the corner algebra to 0.1%. Its self-consistent exponent was stable under wedge truncation, moving 1.3×10^{-5} across the decade $\varepsilon_b = 10^{-4}$ to 10^{-5}, where the ground state moves 2.72×10^{-3} over the same decade. And it carried a coherent morphological signature, an outward-displaced amplitude lobe and a sign-flipped angular harmonic at $6172\times$ the variation of the ground branch. By every test we had been applying, it was a new solution.

7.2 What it was

Under refinement its exponent moved *away* from α_1 with *growing* steps, and toward α_2 and α_3 without contracting on either (Figure 3):

resolution	α	c_ℓ	h_{id}
$(16, 40, 12)$	-0.42172919	5.392	$+2.386$
$(24, 56, 12)$	-0.42554621	4.001	$+0.994$
$(28, 64, 18)$	-0.43083651	3.887	$+0.880$
ground, for scale	-0.34471229	3.005	-0.00106

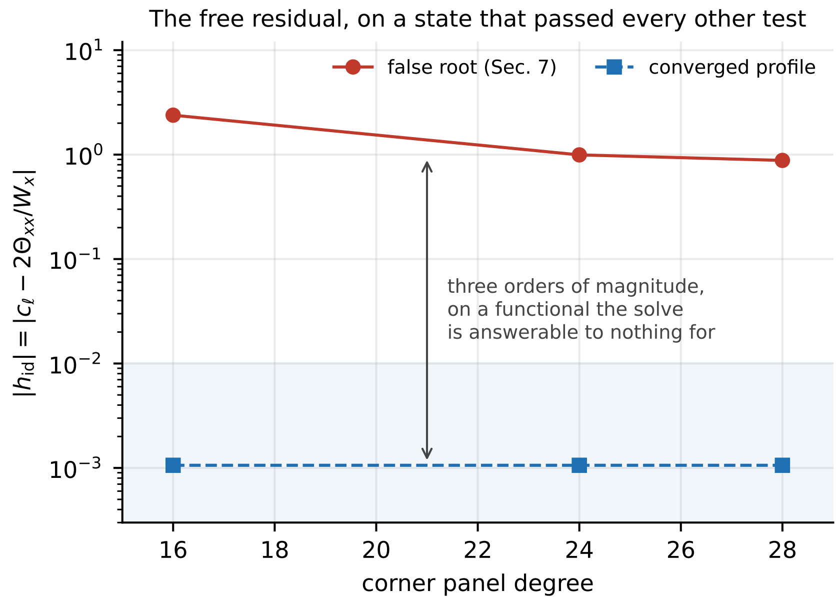

Figure 2: The free residual $|h_{\mathrm{id}}|$ for the converged profile and for the false root, across corner degree. Three orders of magnitude, on a functional neither solve is answerable to, separating two states that agree on every other diagnostic.

The free residual of Section 2.3 is violated by $O(1)$ throughout, three orders of magnitude above the ground state (Figure 2), while every other diagnostic looks healthy. Its distance to α_2 shrinks from 2.23×10^{-2} to 1.31×10^{-2} across the three rungs, which is why we describe the object as drifting rather than diverging, and why an "α_2 in disguise" reading cannot be excluded by these data alone.

7.3 The rescue that failed, and what its failure measured

We tested the natural rescue, that the state is a genuine profile carrying its *own* corner data, by promoting Θ_{xx} to an unknown (W_x absorbs the scaling normalization of Section 5) and closing with the corner identity. The formulation was built and its Jacobian verified to 4.2×10^{-11}, and it failed its ground-state control, which is the informative outcome: the pinned solution family *self-parallels* the identity line, $dc_\ell/d\Theta_{xx} = +1.677$ against the identity slope $2/W_x = +1.672$, a 99.7% cancellation. The corner identity cannot serve as a closure; it is a diagnostic and only a diagnostic. The candidate state then failed from both corner-data seeds, with residuals floored at 2.2 to 2.4×10^{-3}, and a continuation ramp showed the identity defect has no sign crossing anywhere physical, extrapolating to three times the true corner value.

7.4 The lesson

We conclude the state is an artifact of the pinned discretization with no continuum limit, and we state the general form of the lesson: **residual, distinctness under deflation, parameter stability and morphological coherence are jointly insufficient to certify a self-similar profile.** In this instance a free residual separated the cases where those four did not, on a single

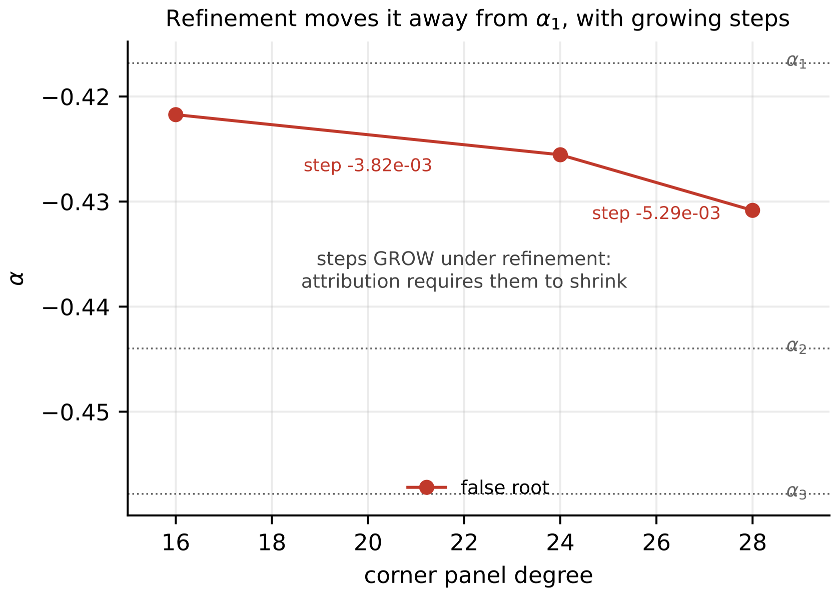

Figure 3: The false root's exponent under refinement, with the published $\alpha_1, \alpha_2, \alpha_3$ marked and the step sizes labelled. Attribution to α_1 requires the steps to shrink; they grow.

artifact, at a cost of one extra line of output. A formulation that pins its gauge to imported corner data can manufacture such a state; we have not seen the failure mode reported.

8 Reproduction and retractions

`polar_cornerreg.py` implements Section 2 and returns h_{id} on convergence. `polar_spectrum.py` implements the Section 6.1 realization and its three gates; the Section 6.2 and 6.3 certificates were computed by separate measurement scripts. The three figures are generated from logged measurements by `repro/scripts/figures.py` with no smoothing and no interpolated points. `ALPHA_RESULT.md` is the full campaign record and `NOTE_CLAIMS.md` grades every claim in this note against its evidence.

Every retraction made during this work is recorded rather than removed: a spectral mode claim built on unconverged eigenvalues; a log-periodic extrapolation refused by model selection; the essential-numerical-range claim retracted above; and a corner-angle derivative $d\alpha/d\theta = +1.40$ per radian, which was the most expensive of the four and was withdrawn when the slope proved formulation-dependent (-2.8 in the panel frame against approximately -30 regularized). We regard the retraction record as part of the result.

Open questions

Four questions stand open. The corner-clamped admissible class of Section 6.3 removes two directions whose dynamical content is unmeasured. The mass matrix $E = I$ on transport rows rests on two independent derivations and a reduction check but not on a third structurally different test; a short time-march compared against e^{tL} on the same perturbation would supply one. The behaviour of ε^* under genuine far-field refinement of the stability operator is untested. And the unstable branches remain unconfirmed by any non-network method, including this one: the route attempted here produced the artifact of Section 7, and a formulation treating α as a Newton unknown with its own normalization on the untruncated problem is the natural next attempt.

References

[1] J. Chen and T. Y. Hou, *Stable nearly self-similar blowup of the 2D Boussinesq and 3D Euler equations with smooth data I: Analysis*, arXiv:2210.07191.

[2] J. Chen and T. Y. Hou, *Stable nearly self-similar blowup of the 2D Boussinesq and 3D Euler equations with smooth data II: Rigorous Numerics*, arXiv:2305.05660; Multiscale Model. Simul. **23**(1), 25–130 (2025).

[3] J. Chen and T. Y. Hou, *Singularity formation in 3D Euler equations with smooth initial data and boundary*, Proc. Natl. Acad. Sci. USA (2025), doi:10.1073/pnas.2500940122.

[4] Y. Wang et al., *Discovery of Unstable Singularities*, arXiv:2509.14185.

[5] Y. Wang, *Singularity Formation: Synergy in Theoretical, Numerical and Machine Learning Approaches*, arXiv:2604.16842 (PhD thesis).

[6] G. Luo and T. Y. Hou, *Potentially singular solutions of the 3D axisymmetric Euler equations*, Proc. Natl. Acad. Sci. USA **111**(36), 12968–12973 (2014), doi:10.1073/pnas.1405238111.